FULL RESEARCH ARTICLE

Efficient utilization of remelt strategy for improving relative density and surface integrity to eliminate necessity of performing post-processing of additively manufactured 316L stainless steel

Sajjad Rajabi[1] · Alireza Khodabandeh[1] · Mohamad Sina Sadeghi[1] · Masood Amirshami[1] ·
Ardeshir Hemasian Etefagh[1] · Mohsen Khajehzadeh[1] · Mohammad Reza Razfar[1]

Abstract

Selective Laser Melting (SLM) is an advanced additive manufacturing method for producing complex metal components. However, post-processing steps are often needed due to the nature of the process. These steps include sandblasting to address high surface roughness and heat treatment to address unintended porosity, microstructural heterogeneity, and hardness fluctuations. These post-processing steps increase costs and production time. Remelting is an alternative method that involves scanning layers without powder recoating, presenting its challenges. In this study, we investigate the effects of remelting parameters and scanning strategies on the surface roughness, relative density, and microstructure of SS316L steel parts manufactured using SLM. The goal is to design an optimal scanning strategy to eliminate the need for post-processing, saving time and reducing costs. The process parameters include the remelting of layers, scan line spacing, and relative rotation angle between two layers. Based on the experimental design using a full factorial approach, 27 samples were printed, with each parameter examined at three levels. The samples were then measured for surface roughness using laser profilometry and relative density using Micro-CT technology. The results were compared with samples subjected to post-processing steps such as sandblasting and heat treatment. The remelting strategy achieved a relative density of 99.12%; moreover, Micro-computed tomography analysis further revealed that the remelting process not only reduced porosity but also led to a notable enhancement in pore geometry, transitioning from crack-like and lack of fusion defects to smaller spherical pores. In terms of microstructure, a more uniform structure and higher hardness between 202 and 207 Vickers were achieved. The remelting strategy was able to reduce the surface roughness within the range of 7 μm. Some challenges posed by remelting, such as compatibility with other parameters, the significantly longer time required for remelting of all layers, and overmelt, were examined and addressed in the discussion.

Keywords Selective laser melting · Surface roughness · Relative density · Micro-hardness · Remelting strategy

✉ Mohsen Khajehzadeh
  mo.khajehzadeh@aut.ac.ir; mo.khajehzadeh@gmail.com

Sajjad Rajabi
  sajjad.rajabi@aut.ac.ir

Alireza Khodabandeh
  alz.khodabandeh@aut.ac.ir

Mohamad Sina Sadeghi
  msinasadeghi@gmail.com

Masood Amirshami
  masood.a.shami@gmail.com

Ardeshir Hemasian Etefagh
  hemasian@aut.ac.ir

Mohammad Reza Razfar
  razfar@aut.ac.ir

1   Department of Mechanical Engineering, Amirkabir
    University of Technology, Tehran, Iran

🙼 Springer

1 Introduction

Selective Laser Melting (SLM) is an additive manufacturing process that utilizes a high-powered laser to selectively fuse metal powders, layer by layer, to create complex three-dimensional objects [1–3]. Notably, 316L is a widely utilized material in SLM due to its advantageous characteristics such as resistance to corrosion, weldability, machinability, and cost-effectiveness [4–8]. However, despite its advantages, the process is not without its challenges, which have spurred the attention of researchers who are actively engaged in addressing these limitations.

Porosity is a significant concern in selective laser melting (SLM) and poses challenges to the mechanical properties and performance of the manufactured parts. During the SLM process, the localized melting and solidification of metal powder layers can lead to the entrapment of gas within the material, also insufficient in fusion resulting in the formation of pores called Lack of Fusion. These pores can act as stress concentrators, weakening the structural integrity and reducing the strength and fatigue resistance of the parts [9]. Post-processing techniques are commonly employed to mitigate the issue of porosity [10]. One such technique is heat treatment, which involves subjecting the SLM parts to elevated temperatures for a specific duration [11–13]. Heat treatment promotes the diffusion of gas atoms and the rearrangement of solidification defects, leading to a reduction in porosity [14–16].

In SLM, achieving a high surface quality can be challenging due to the nature of the process. The layer-by-layer melting and solidification of the metal powder can result in surface roughness, stair-stepping effects, and visible defects [17]. These surface imperfections can limit the use of SLM parts in applications where a smooth and aesthetically appealing finish is required [18, 19]. Post-processing steps such as sand-blasting or polishing are often employed to improve the surface quality and dimensional accuracy of the parts [20]. Laser re-melting can be employed as a method to achieve surface smoothing without the need to remove the part from the construction platform. This approach effectively prevents any fixation faults that may occur with the existing SLM equipment [19, 21].

Variations in micro hardness within metal parts can have significant implications for their performance and durability. Inhomogeneities in micro hardness can lead to localized areas of lower strength, creating weak points within the part. As a result, when different regions with varying micro hardness expand or contract at different rates, it can cause the part to distort, warp, or undergo dimensional changes. To address this issue, heat treatment is frequently employed to even out the hardness and microstructure, making them more consistent throughout the part [22–26].

By optimizing the main parameters or scan strategy, it is feasible to reduce the requirement for certain post-processing operations in selective laser melting. However, achieving a complete elimination of post-processing remains a challenge that has yet to be overcome. While there is a wealth of research focused on optimizing the main process parameters for each specific material, there is also a need to consider the optimization of scan strategies to further enhance part quality [27]. To overcome these issues, remelting strategies have been developed to improve the quality of SLM parts. Remelting involves melting a layer of the part again using a laser or electron beam [28–32].

While the remelting layers strategy has shown promise in improving the porosity and surface roughness of selective laser melted (SLM) parts, there are several challenges and limitations associated with its implementation.

The primary concern pertains to the scalability and efficiency of the process. Remelting layers can be a time-consuming and labor-intensive process, especially when applied to complex or large-scale SLM parts. Scaling up the process for industrial applications may pose challenges in terms of productivity and cost-effectiveness [33, 34].

The remelting process involves localized heating of the surface, which can create significant thermal gradients within the part. High thermal gradients can result in residual stresses and distortion, which may affect the dimensional accuracy and overall integrity of the part [33, 34].

Additionally, achieving optimal remelting parameters, such as laser power, scanning speed, and hatch distance, is of paramount importance, as it poses significant challenges in terms of controlling these parameters effectively It requires precise control to ensure the desired level of porosity reduction and surface finish improvement without causing adverse effects, such as excessive melting or overheating [34, 35].

QIU found that remelting could lead to smoother surfaces and eliminate pores in the uppermost layer. Moreover, sufficient remelting resulted in good bonding at interlayer interfaces [36].

Yasaa discusses the use of laser re-melting as a solution to improve surface quality and reduce residual porosity in Selective Laser Melting (SLM) parts. They show that laser re-melting resulting in longer production times. Additionally, it is stated that nearly all components subjected to laser remelting exhibited a higher microhardness when compared to a reference component manufactured using SLM [21, 37].

Yu performs re-melting strategies and also rescanning the direction of the laser on the AlSi10Mg parts, generating significant reductions in surface roughness and porosity [38].

However, most researchers only paid attention to rescanning all the layers of parts. There was little literature related to the effect of rescanning with reduced interlayer times.

Ma explored the solidification characteristics of molten pools by suggesting a merged rescanning approach and

Table 1 Chemical composition of stainless steel 316L

Elements	Fe	Ni	Si	S	P	Mn	C	Mo	Cr
Wt.-%	Balance	13.8	0.8	0.03	0.045	1.1	0.04	2.6	17.3

doing finite element analysis. Testing different rescanning procedures and process parameters allowed for the production and analysis of Ti6Al4V alloy specimens. This research looks at the size, relative density, and microstructure of pore flaws using various rescanning techniques. According to their findings, the average cooling rate was graded as follows: SLM > re-SLM + IL1 > re-SLM. The results show that rescanning without layer intervals achieves the best relative density and optimization of residual stress [33].

In summary, the literature review underscores the potential of remelting as a viable alternative to post-processing in Selective Laser Melting (SLM). By studying the results of several scanning procedures and remelting settings, it becomes evident that remelting offers promising prospects for reducing surface roughness, enhancing relative density, and achieving a more uniform microstructure. Despite the challenges associated with remelting, ongoing research endeavors aim to optimize the process and expand its applicability in SLM-based manufacturing. Further research is warranted to fully exploit the benefits of remelting and advance additive manufacturing capabilities. In this project, "Skip Layer Remelting" is explored to reduce scanning time, and compatible remelting parameters are introduced. Finally, the results are compared with post-processed samples in terms of surface roughness and relative density to assess the feasibility of replacing post-processing steps with remelting.

2 Materials and methods

2.1 AISI 316L powder preparation

This article utilizes 316L powder from Noura company, which is produced using the atomization method. The composition percentage of this powder is provided in Table 1. The particle size of the powder falls within the range of 15 to 45 microns, as shown in Fig. 1.

2.2 Design of experiments table

Due to the need for a comprehensive and independent examination of each factor in the subject, the experiment was designed as a full factorial design. In this design model, only one of the levels related to a parameter change in each sample, while the remaining parameters remain constant to ensure that the experimental result is entirely a function of the changed parameter value. Therefore, using the full
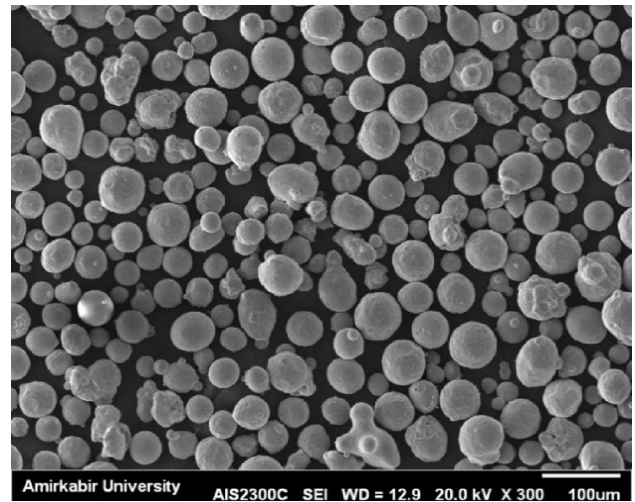
Fig. 1 SEM image of SS316L powder

Table 2 Defined levels for each process parameter

Parameters	Levels		
	1	2	3
Remelt	N/A	Every Other Layer	Each Layer
Hatch space (μm)	40	60	80
Layer rotation (degree)	10	50	90

Table 3 Optimal numerical values of the printing parameters for SS316L steel

Parameters	Laser power (W)	Scan strategy	Scan speed (mm/s)	Layer thickness (μm)	Square size (mm)
Optimal values	180	Chessboard	1200	30	5

factorial method outlined in Table 2, the effects of process parameters have been investigated.

Furthermore, the optimal constant values for other parameters were used for this powder material (Table 3). We utilized the optimized parameters from a referenced article and acknowledged their work. Also, these parameters were within the range of optimized parameters suggested by the Noura company for 316L powder [39], which is the manufacturer of SLM machine that is used in this study.

To control and reduce thermal gradients in the melt pool, remelting was performed at a power of 100 in all samples. Additionally, to decrease printing time, the laser scanning speed during remelting was increased to 2000 mm per second.

Table 4 provides information on the number of samples, their corresponding parameters, the relative density and roughness average of the samples both before and after undergoing sand blasting.

The samples were printed in the form of a rectangular cuboid with dimensions of 10×10×4 mm using the M100P Noura printer. The diameter of the laser focal spot is 80 μm. The parts are printed in a chamber filled with argon gas to prevent oxidation and contamination. The device is powered by a 200–220 V source and operates with a current of 32 A.

Furthermore, this device does not have the capability of remelting individual layers. Therefore, an algorithm was designed to not only enable this capability but also allow for skip layer remelting during the remelting process. The method is as follows: the initial sample design is performed with the specified parameters, and then a remelting-specific piece is designed to be identical in dimensions to the initial sample. both pieces are precisely aligned together in the device's software, so when the laser scans, it scans both pieces in the same layers. As a result, the remelting parameters can be fully adjusted, and custom layer selection for remelting is also possible. Figure 2 presents a diagram that helps enhance comprehension of hatch spacing, rotation, and the process of remelting all layers, as well as every other layer.

2.3 Surface roughness analysis

Surface roughness is a mechanical property of materials that is defined as the deviation of a real surface from its average value along a vector perpendicular to the surface. The lower the deviation, the lower the surface roughness, indicating fewer peaks and valleys on the surface. Conversely, higher deviation indicates the presence of more peaks and valleys, resulting in higher surface roughness. The surface roughness analysis was conducted using a laser profilometer, LPM-D1, with an accuracy of ± 1 μm,

Table 4 Sample numbering, surface roughness, and relative density results

Sample No	Hatch space (μm)	Rotation (degree)	Remelting	Density (%)	Ra (μm)	Ra (Sand blast) (μm)
1	40	10	N/A	95.29	13.7	11.2
2	40	10	Each layer	98.36	8.4	
3	40	10	Every other layer	99.12	9.1	
4	40	50	N/A	95.56	15.4	12.5
5	40	50	Each layer	94.13	7.2	
6	40	50	Every other layer	94.87	9.6	
7	40	90	N/A	90.01	13.8	11.9
8	40	90	Each layer	91.91	8.9	
9	40	90	Every other layer	93.14	9.4	
10	60	10	N/A	95.69	13.7	11.4
11	60	10	Each layer	96.24	9.2	
12	60	10	Every other layer	98.83	9.8	
13	60	50	N/A	93.51	14.4	11.9
14	60	50	Each layer	94.76	11.5	
15	60	50	Every other layer	95.89	8.9	
16	60	90	N/A	91.47	15.3	12.5
17	60	90	Each layer	89.95	10.9	
18	60	90	Every other layer	91.32	10.8	
19	80	10	N/A	95.11	16.7	12.6
20	80	10	Each layer	94.46	8.3	
21	80	10	Every other layer	94.88	11.7	
22	80	50	N/A	93.23	18.7	13.1
23	80	50	Each layer	95.19	10.4	
24	80	50	Every other layer	95.04	8.9	
25	80	90	N/A	89.09	15.9	12.5
26	80	90	Each layer	92.34	9.6	
27	80	90	Every other layer	91.06	12.4	

Fig. 2 Schematic for better understanding of **A** Remelting and **B** Hatch Spacing and relative angular rotation between layers
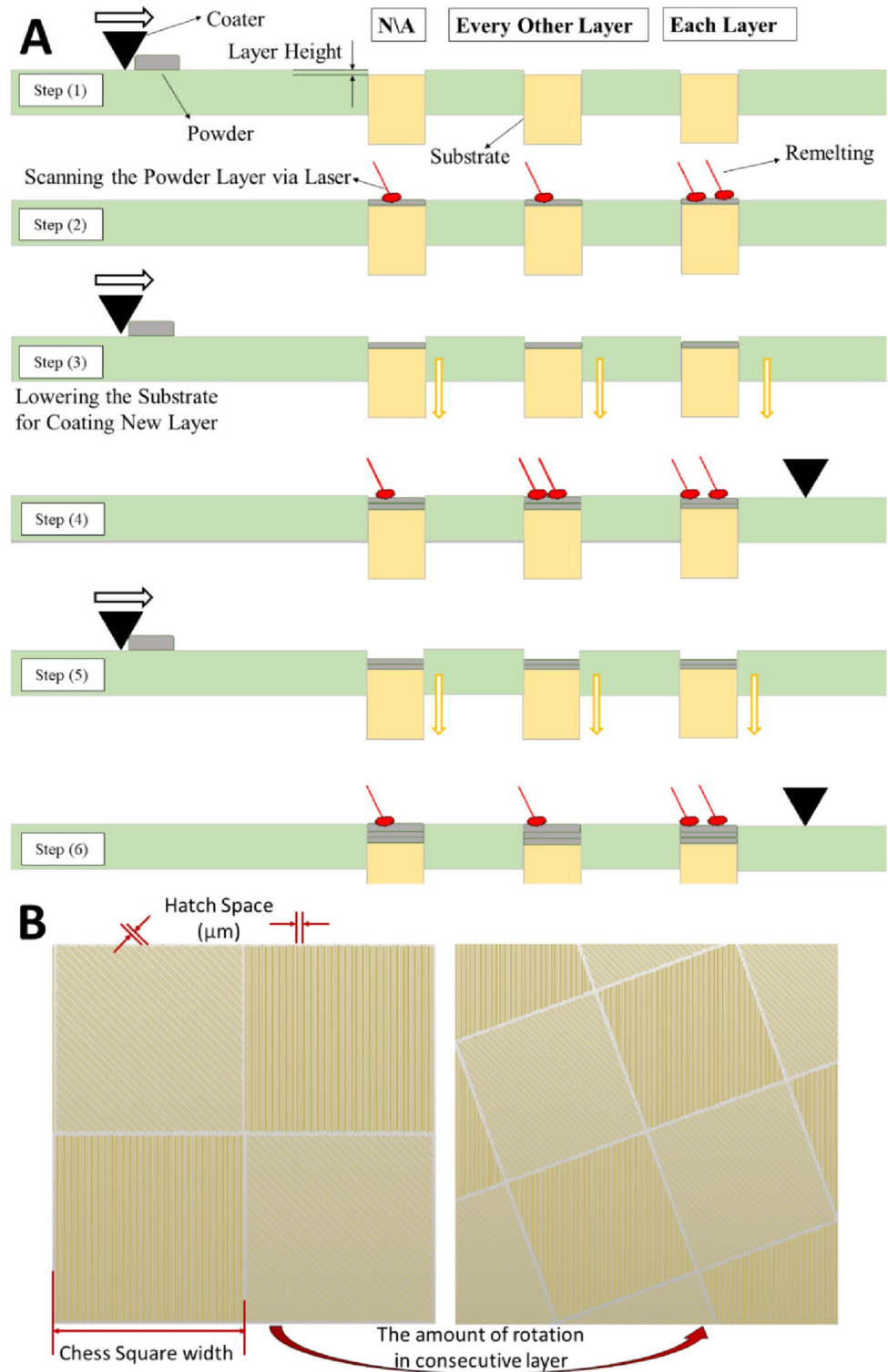
in the form of scanning 2×2 mm square areas. Sandblasting was performed on the non-remelted samples for comparison with the remelted samples.

2.4 Microstructure and microhardness analysis

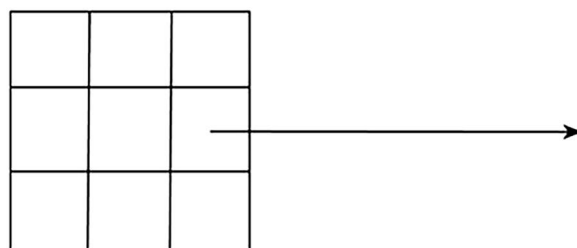To achieve microstructure homogenization and hardness, annealing heat treatment was performed on the non-remelted

samples numbered 1, 4, 7, 10, 13, 16, 19, 22, and 25 at a temperature of 1100 degrees Celsius for two hours under vacuum conditions, followed by furnace cooling. Subsequently, all samples underwent a 15-s etching process using Marble as the etchant solution.

The microhardness of the re-polished samples was assessed using a Shimadzu-type M microhardness tester device. This device employs the Vickers method (HV0.05) to evaluate the hardness of the samples under standardized conditions, including an applied load of 50 g and a dwell time of 10 s. To ensure a comprehensive analysis, the surface of each sample was divided into nine sections. Within each section, the microhardness of 12 points was randomly measured. (Fig. 3) Consequently, a total of 108 points of microhardness were measured for each sample. Subsequently, a 2D contour of microhardness was generated based on these results, providing a detailed visualization of the hardness distribution across the sample surfaces. This methodology allows for a thorough examination of the hardness characteristics of the re-polished samples, facilitating a deeper understanding of their mechanical properties.

2.5 Measurement of relative density and pore analysis

One of the best and most accurate methods for calculating porosity is the utilization of high-resolution X-ray tomography imaging or Micro-CT images. X-ray tomography imaging is based on the absorption of X-rays by different materials. In this study, the LOTUS NDT Micro-CT device, manufactured by Behin Negareh, was employed with a resolution of one micrometer. Additionally, two-dimensional SEM images were obtained and metallographic images were captured using a microscope. The samples subjected to heat treatment and remelting were investigated in terms of porosity and relative density.

3 Results and discussion

3.1 Surface roughness analysis

The effect of parameters on the surface roughness of the samples is investigated from two perspectives. The first perspective involves analyzing the results obtained from mathematical modeling using the full factorial method and analyzing the graphs. The second perspective involves the physical and mechanical analysis that applies to each sample in the melting zone. Based on previous research results and an understanding of the physical conditions governing the process, the impact of each parameter can be examined in terms of creating different conditions in the melting zone and the particle bonding mechanism.

To evaluate the level of conformity between the model and real-world observations, the analysis of variance (ANOVA) and Pareto plot techniques (Fig. 4) were employed. These analyses generated tables that quantified the magnitude of the effect associated with each parameter. The ANOVA and Pareto plot analyses allowed for the assessment of parameter significance concerning the model's alignment with reality. These analytical tools
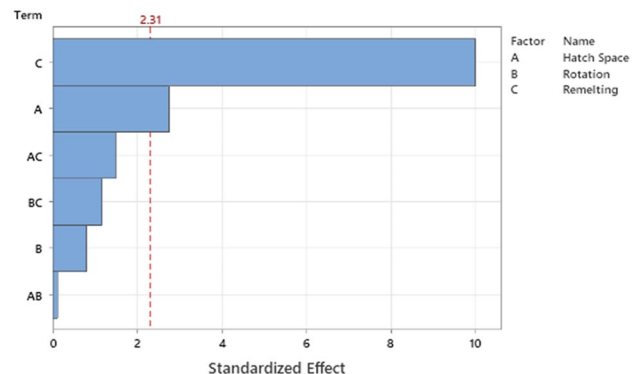

Fig. 4 Pareto charts of the standardized effects for surface roughness

Fig. 3 Microhardness measurement details

provided valuable insights into the relative influence of each parameter and their relevance in relation to the study's objectives.

The ranking of parameters based on their significance is calculated using the *P* value coefficient. A parameter with a lower *P* value is considered more influential. Therefore, Table 5 indicates that the most influential parameter on surface roughness is remelting, followed by the hatch spacing, and finally the rotation. Considering the calculated *P* values for each parameter, it can be observed that these values for remelting and hatch spacing are below 0.1, indicating a 90% confidence level in their effectiveness on the experimental results. The effect of remelting on surface roughness is clearly visible to the naked eye in Fig. 5.

The value of the R-Squared (R-Sq) parameter indicates the accuracy of the modeling and how well the model matches reality. A higher value signifies that a greater portion of the obtained results are justified by the developed model. In this experiment, an R-Sq value of 95.5% was achieved. This value implies that 4.5% of the experimental results cannot be explained by the analysis provided in the full factorial model. As evident in the statistical analysis, the effects of parameters cannot be regarded as independent factors on surface roughness. Each parameter, when its value changes, introduces a variation in the powder melting process. Whether this variation is beneficial or detrimental to surface roughness depends on the conditions imposed by the other parameters in the melting process. Therefore, the effects of parameters are interdependent on each other.

According to the results of ANOVA, the rotation parameter had the least impact on surface roughness. In terms of the powder melting process analysis, it does not have a significant influence on the formation of the melt pool on the material surface. However, it plays a crucial role during the printing process. Therefore, the rotation parameter is considered the most important factor influencing relative density. A detailed analysis of the relative density results will be further discussed in the context of the relative density analysis. Therefore, for easier analysis of the
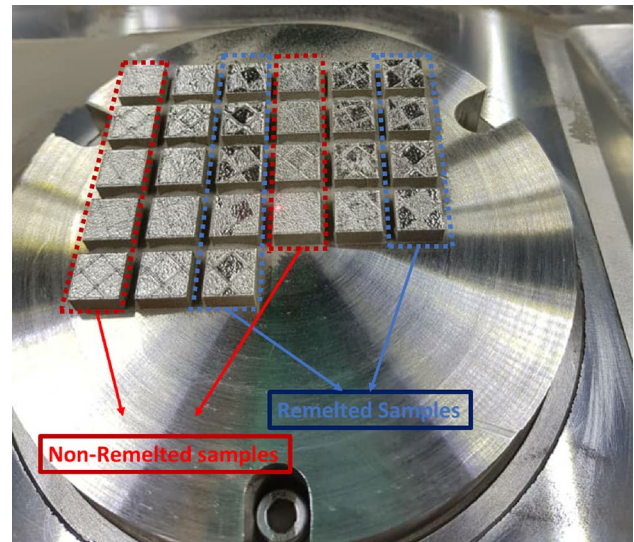

Fig. 5 Photo of the printing table and printed samples

parameters of hatch spacing and remelt in the intersecting graphs, the rotation parameter is kept constant at a fixed level, and the graphs of Fig. 6 are analyzed.

As mentioned earlier, the remelt parameter has the greatest impact on surface roughness. Even with every other layer remelting, a significant improvement in surface roughness is observed. For example, samples 1 and 3, which have the same hatch spacing and rotation parameters but differ only in the presence of every other layer remelting, show a surface roughness improvement from 13.7 to 9.1 μm, indicating a 4.6 μm improvement in surface roughness.

The scan line spacing parameter has an inverse relationship with laser overlap in the two scan paths. The focused laser diameter is 80 μm, so it covers the entire scan path on all the specified surfaces. Increasing this parameter from 80 μm may result in the presence of un-melted powder. Conversely, reducing this value increases the laser overlap in the two closely spaced scans on the surface, creating a similar effect to remelting in that region.

Table 5 ANOVA of full factorial model for surface roughness results

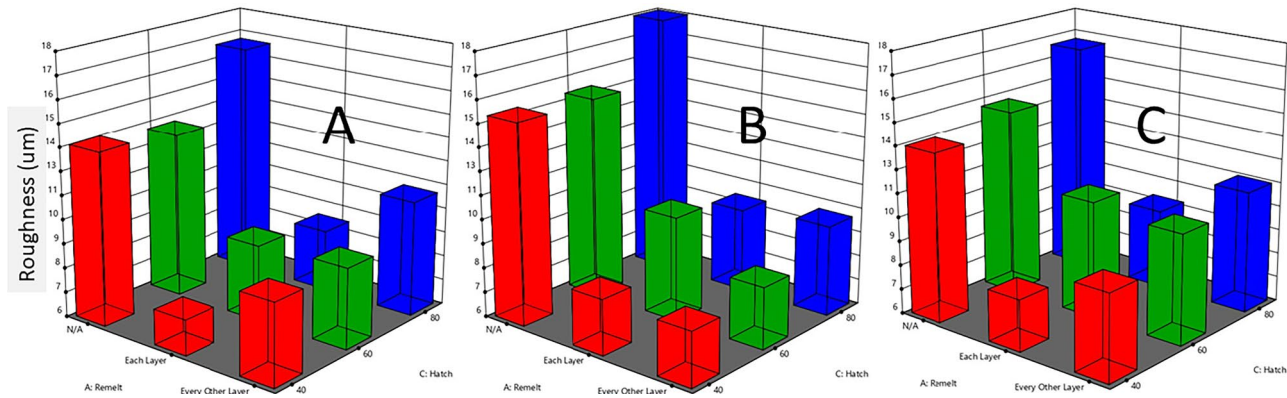| Source	Sum of squares	df	Mean Square	*F* value	*P* value	
Model	227.48	18	12.64	9.42	0.0015	Significant
A-Remelt	188.06	2	94.03	70.10	<0.0001	
B-Rotation	2.38	2	1.19	0.8880	0.4485	
C-Hatch	16.26	2	8.13	6.06	0.0250	
AB	8.32	4	2.08	1.55	0.2767	
AC	11.20	4	2.80	2.09	0.1743	
BC	1.25	4	0.3128	0.2332	0.9120	
Residual	10.73	8	1.34			
Cor total	238.21	26				

Fig. 6 Surface roughness graphs based on the variables Hatch and Remelt with constant parameters **A** Rotation 10, **B** Rotation 50, and **C** Rotation 90

In Fig. 6, it can be observed that reducing the hatch spacing, although having a minor impact on the results, has still improved the surface roughness. Hatch spacing of 80 μm, chosen to minimize laser overlap, may result in a significant amount of un-melted powder remaining on the surface of the part. Additionally, the combined effect of remelting and scan line spacing can be seen, where remelting has been able to fill the gaps left by wider hatch spacing. For example, in samples 20, 23, and 26, despite having a hatch spacing of 80 μm, the surface roughness was reduced due to the remelting process. It is possible that in the first scan, although there is less laser overlap and some un-melted powder is present, this deficiency has been compensated for in the second scan. In Fig. 7, microscopic images of the surface and corners of the samples without polishing are shown, as well as the surface roughness of the "No-remelted" and "Remelted" samples.

As observed, on the surface of the sample without remelting, some surface defects such as voids can be seen. These defects have been largely eliminated by the remelting process, justifying the lower surface roughness of the sample. Additionally, the SEM images of un-melted powders obtained from the sides of the "No-Remelted" sample provide clear visual evidence regarding the formation of voids called Lack of fusion.

When a number of incompletely melted powder particles are placed next to each other, they create voids known as Lack of Fusion (LOF). The size and quantity of these voids vary depending on the size and number of incompletely melted powders, extending into the interior of the component.

In the Remelted sample, the powder particles have partially merged within the component, contributing to improvements in both surface smoothness and density. Although this observation is evident in the SEM images, a numerical analysis of the surface roughness of the sample

corners indicates that the remelting process had a limited effect. The surface roughness values exhibited an alternating pattern, which is attributed to the layer-by-layer nature of the process. It suggests that changes in strategies, such as remelting, have a greater impact on the surface perpendicular to the scanning direction, where the melt pool is involved.

Upon examining the surface roughness of the samples after sandblasting, it became evident that this post-processing operation has the capability to reduce the surface roughness to some extent, with an approximate range between 11 and 13 μm. Sample 7 exhibited the least reduction in roughness (1.7 μm), while sample 22 showed the highest reduction (5.6 μm). It is worth noting that the remelting process has been significantly more effective in reducing surface roughness compared to sandblasting.

The best sample with the lowest surface roughness is sample number 5, with a roughness of 7 μm. It possesses remelting parameters throughout all layers, a hatch spacing of 40 μm, and a rotation of 50 degrees. On the other hand, the sample with the highest surface roughness is sample number 22, with a roughness of 19 μm. This sample has hatch spacing of 80 μm, a rotation of 50 degrees, and no remelting performed.

3.2 Relative density

Similar to the surface roughness experiment, the analysis of variance (ANOVA) table in Table 6 and Fig. 8 is also referred to for examining the magnitude of the effect of each parameter on relative density.

According to this table, the parameter for rotation had the most effect on relative density, even if it had no impact on surface roughness outcomes. Following that, the remelting parameter has an important role in porosity.

In this experiment, the R-Squared value is obtained as 91.89%, which is considered a good value. In this section,
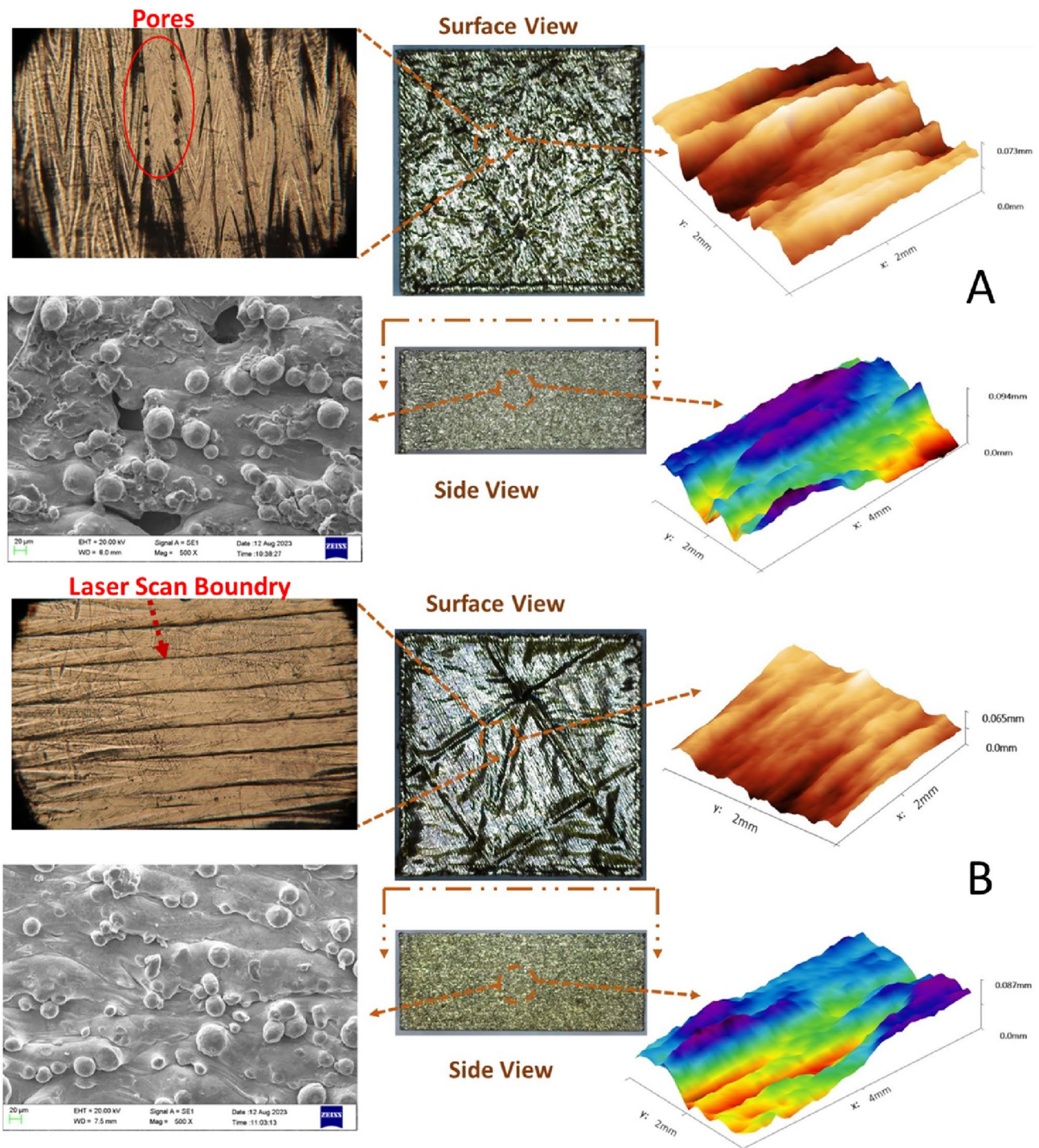
Fig. 7 Microscopic images and laser profiles of the surface and side of the sample without polishing, labeled as **A** No-remelted, and **B** Remelted

Fig. 9 and Fig. 11 are used to demonstrate the individual and simultaneous effects of the parameters on relative density. Finally, the justification of the results is examined based on SEM and micro-CT images.

By increasing the rotation parameter, the relative density has significantly decreased. For example, in samples 1 to 7,

11 to 17, and 2 to 8, which have the same values for the other two parameters and differ only in the increased rotation, we observe a decrease in relative density by 5.28%, 6.29%, and 5.54%, respectively. This reduction in relative density is quite noticeable in the metal 3D printing process, where achieving high-density prints is one of its strengths. In the

Table 6 ANOVA of full factorial model for relative density results

Source	Sum of Squares	df	Mean Square	F value	P value	
Model	162.92	18	9.05	5.04	0.0126	Significant
A-Remelt	12.86	2	6.43	3.58	0.0775	
B-Rotation	131.15	2	65.57	36.50	<0.0001	
C-Hatch	8.11	2	4.05	2.26	0.1671	
AB	1.16	4	0.2911	0.1621	0.9518	
AC	3.64	4	0.9099	0.5066	0.7330	
BC	6.00	4	1.50	0.8357	0.5391	
Residual	14.37	8	1.80			
Cor Total	177.30	26				
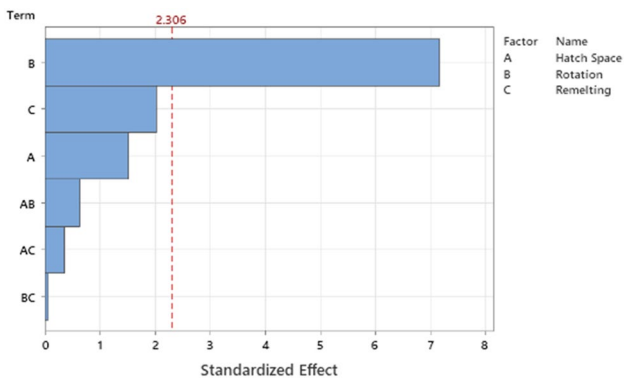
Fig. 8 Pareto charts of the standardized effects for Relative Density

following, this decrease in relative density will be examined by analyzing the surface images of the samples (Fig. 9). The mechanism of rotation angle has been explained according to Fig. 2. According to this pattern, in a relative rotation angle of 90 degrees, there is no significant difference in the overall chessboard strategy, except for the black and white squares swapping their positions. Therefore, during the process with a rotation of 90 degrees, the laser follows nearly the same path in all layers, and the melt pool does not become uniform, especially at the borders of the squares within the chessboard strategy. This flaw may not be apparent in the initial few scanned layers, but as the number of layers increases, the non-uniformity of the melt pool becomes more pronounced, as clearly seen in Fig. 10, even to the naked eye.

As observed, the boundaries of each square in the chessboard pattern are prominently discernible in samples with a rotation of 90 degrees. Similarly, in samples with a rotation of 50 degrees, although with reduced diameter, these boundaries remain perceptible. These distinct boundaries serve as preferential sites for crack initiation and propagation. Conversely, in samples with a rotation of 10 degrees, the boundaries of the chessboard pattern appear significantly fainter and shallower. This can be attributed to the increased number of layers required for the chessboard squares to reach their first position again, thereby resulting in a more homogeneous melt pool.

The impact of remelting can be observed in the graphs of Fig. 7, where in most experiments, it leads to an increase in relative density and consequently a decrease in porosity. Additionally, a decrease in hatch spacing results in increased relative density in most experiments. However, these results have occasionally shown exceptions, which will be further examined using Fig. 11 for investigation.
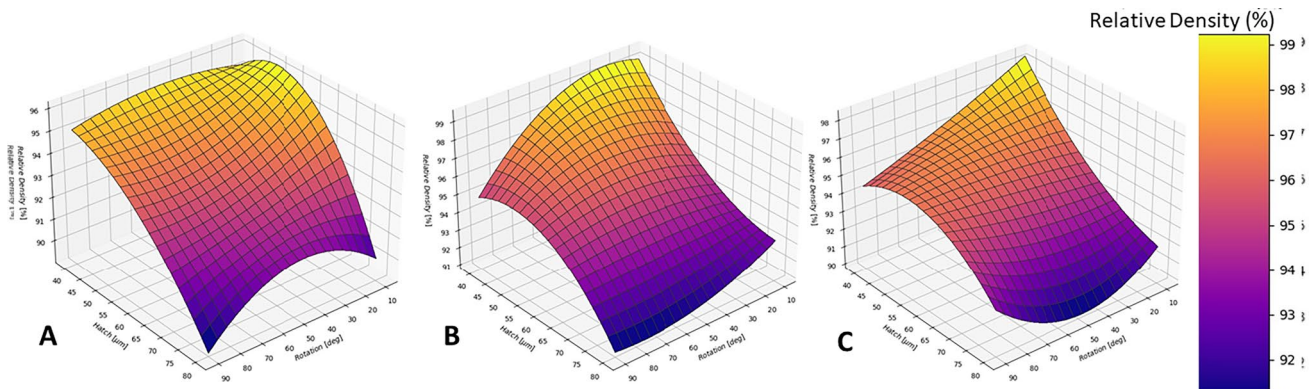

Fig. 9 Relative density plots based on the variables of layer rotation and hatch spacing for the following parameters: **A** Each Layer Remelted **B** Every Other Layer Remelted **C** No Remelted Sample

Fig. 10 Images of sample surfaces captured by the camera with column parameters **A** Rotation 10, **B** Rotation 50, and **C** Rotation 90
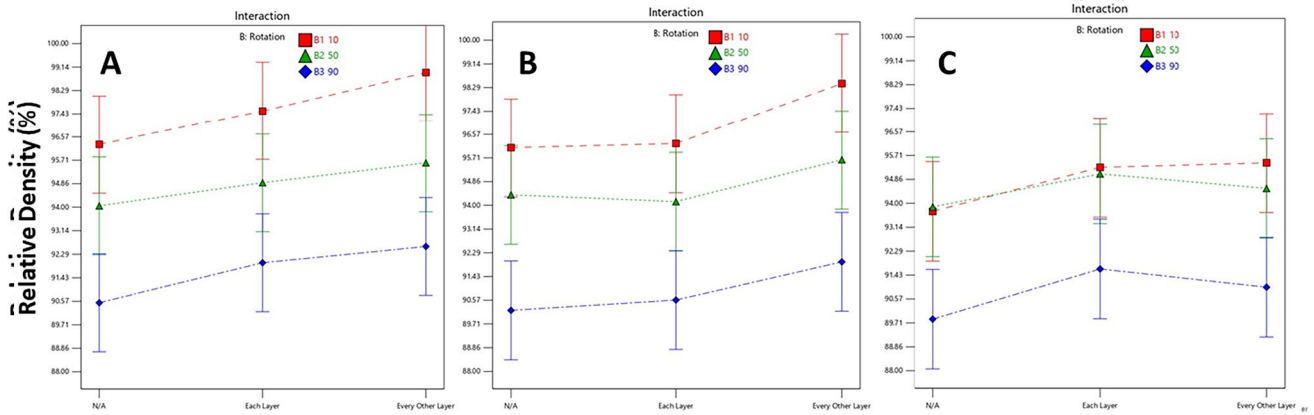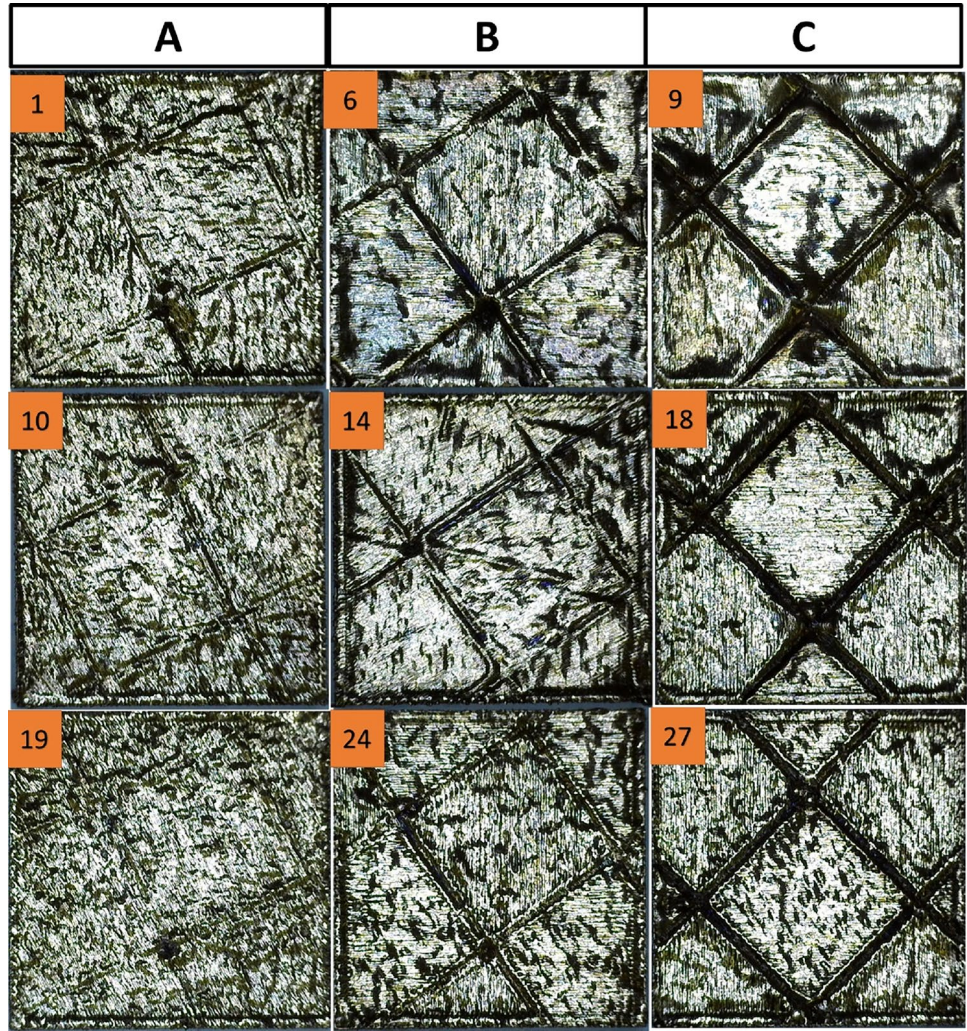

Fig. 11 Relative density plots based on the variables of remelting and relative rotational angle with a fixed parameter: **A** Hatch 40, **B** Hatch 60, **C** Hatch 80 μm

By examining Fig. 11, it becomes evident that despite the positive influence of remelting on relative density results, it was observed that when the hatch spacing was set to 40 (Graph A), each layer remelting had a negative impact on relative density compared to every other layer remelting. This could be due to the fact that at a smaller

hatch spacing, although there is increased laser overlap and un-melted powders that have not reached sufficient heat are eliminated, the generated heat is also increased. Especially when scanning the same layer with low hatch spacing again, this phenomenon is greatly magnified, leading to the heightened presence of defects caused by excessive heat, such as gas bubbles. To confirm this observation, the hatch spacing parameter is consistently set to 60 μm, and Graph B is analyzed and Consistent outcomes are observed in this graph as well. The examination of Graph C, with an 80-μm hatch spacing it is found that remelting all layers with an 80-μm hatch spacing achieves a state of equilibrium. Remelting all layers results in higher relative density compared to every other layers. Therefore, while it can be concluded from these graphs that remelting always leads to an increase in relative density, finding a balance between this parameter and other variables, even those that were constant in this study, such as scan power, scan speed, etc., is crucial. This is because remelting every other layer leads to significant savings in time, electricity, and energy costs, as well as the argon gas used in the chamber, and it may also result in improved outcomes.

In general, without considering the simultaneous impact of parameters, remelting at both defined levels has led to an improvement in relative density. This assertion is further supported by SEM and micro-CT images. The densest thermal treatment sample, the sample subjected to remelting, and the sample without remelting were compared to each other in terms of porosity and cavity geometry.

Figure 12 illustrates the porosity resulting from lack of fusion (LOF). The formation mechanism of these defects occurs when some powder particles fail to fully melt and, when they accumulate together, these types of defects emerge within their midst. Given that the powder particle size ranges from 15 to 45 μm, the size of these voids may start from a minimum of 15 μm. The extent of these defects can vary depending on the amount of unmelted powders accumulated together, making them elongated and wider in shape. As observed in Fig. 12, LOF defects can sometimes be elongated, which can significantly reduce the mechanical strength of the component. However, in the samples subjected to remelting, these defects are much less prevalent. The Heat-treatment (annealing) shows potential in mitigating gas porosity; however, due to the incomplete melting of the sample during this particular post-processing stage, a substantial presence of LOF defects is observed.

The SEM and micro-CT images reveal that remelting not only eliminates LOF resulting from insufficient heat but also, due to its stabilizing effect on the molten pool and the prolonged cooling time of the molten pool, allows for a longer duration for gas bubbles to escape. Consequently, these bubbles have more time to rise and exit as the molten pool homogenizes through subsequent scanning. Figure 12

demonstrates that the remelted sample exhibits the least amount of both LOF and balling cavities.

Sample 3, which underwent a remelting process on every other layer, a 10-degree rotation, and a hatch spacing of 40 μm, exhibited the highest relative density among the samples. In contrast, sample 25, which had a rotation parameter of 90 degrees, a hatch parameter of 80 μm, and no remelting treatment, displayed the lowest relative density.

3.3 The geometry and quantity of pores

As previously mentioned, while the micro-CT images provided some insight into the pore geometry, they did not allow for a comprehensive analysis of parameters such as the size of all pores and their sphericity or elongation. In this regard, all pores were analyzed using Avizo software, and a dedicated algorithm was employed to calculate and provide detailed information regarding the number, diameter, and geometry of all pores. The first step in obtaining the equivalent diameter for each pore is calculated using the following formula.

$$\text{Eq\_Diameter} = \sqrt[3]{\frac{6 \times \text{Volume3D}}{\pi}}$$

The first and most straightforward conclusion drawn from these graphs (Fig. 13) is the significantly higher frequency of pores in the No-Remelted sample (329 pores) compared to the Remelted sample (161 pores). The presence of pores with a diameter between 0 and 15 μm in each graph can highly likely be attributed to gas bubbles or ballings. This is because the particle size of the powder used starts from 15 μm, indicating that the minimum size for cavities or LOFs is 15 μm.

Similar to the results obtained from SEM images, the Remelted sample not only lacks elongated cavities or their minimal count but also exhibits fewer gas bubbles. This can be attributed to the longer melting time of the molten pool during the scanning process, allowing more time for the escape of gas bubbles. Consequently, the sample subjected to the remelting process has lower number of small-sized pores compared to no-remelted sample. Additionally, upon examining larger-sized cavities, the Remelted sample exhibits the lowest count, followed by the Heat-Treated sample.

The sphericity of a cavity is also calculated using the following formula:

$$\Psi_{\text{Sphericity}} = \frac{\pi^{\frac{1}{3}} \times (6V)^{\frac{2}{3}}}{A}$$

where V represents the volume of the cavity and A denotes its surface area, and the resulting value falls between zero and one. If this value is equal to 1, it indicates that the cavity is a perfect sphere. The further this parameter is from

Fig. 12 Images of the micro-CT and SEM front and back views of the samples **A** No-Remelted, **B** Remelted, and **C** Heat-Treated
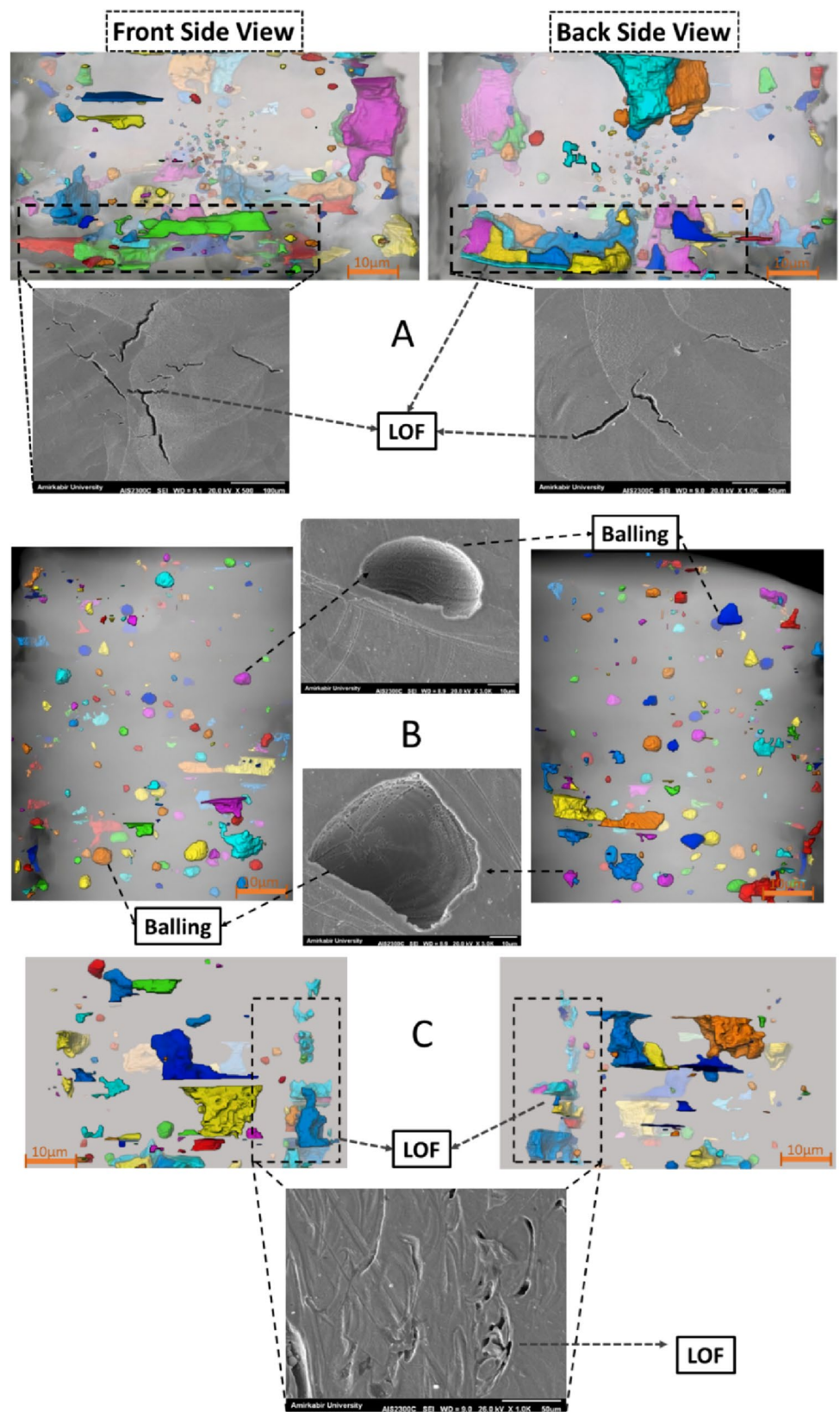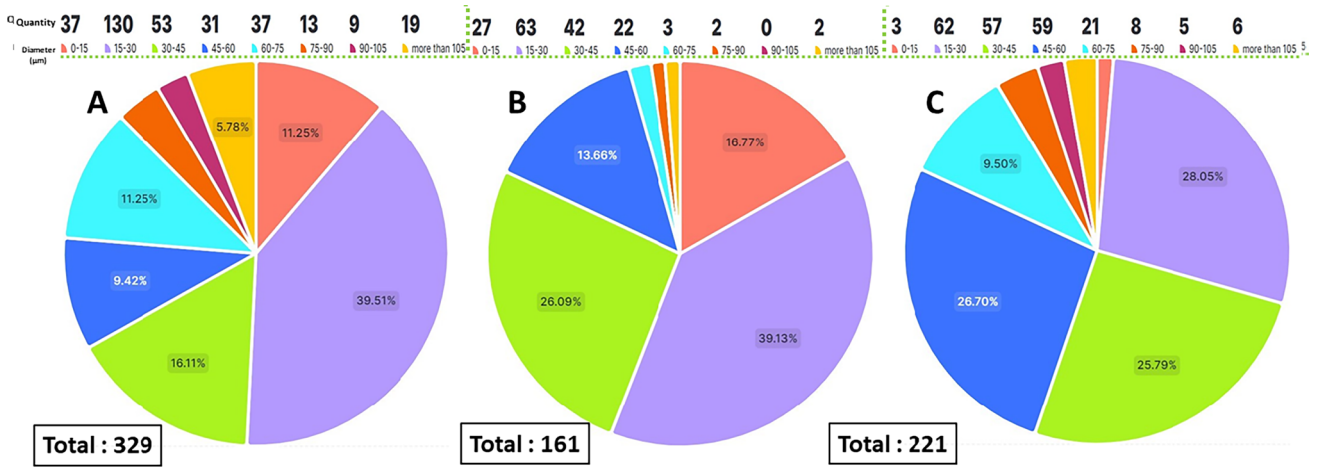
Fig. 13 The quantity of pores based on their equivalent diameter is evaluated in three different samples: **A** (No-Remelted), **B** (Remelted), and **C** (Heat-treated)

one, the more elongated the cavities are. Figure 14 displays the outcomes of the sphericity of pores, categorized according to their equivalent diameter. The computed sphericity for small pores may exceed one, as the 3D surface area is estimated using kernel approximations, providing a more accurate approximation. However, this does not hold true for 3D volume measurements, which do not involve any approximations.

These graphs provide similar results, indicating the high effectiveness of heat treatment in reducing smaller and spherical cavities while being less effective in eliminating elongated and larger cavities. As mentioned before, this is due to the inability to reach the melting temperature during the process. The Remelted sample also predominantly exhibits cavities of the Balling and gas types.

Furthermore, comparing the equivalent diameter plots based on sphericity reveals a crucial point that spherical pores are generally found in smaller dimensions, while cavities of the LOF or elongated type are more prevalent in larger diameters. It should be noted that the specific mechanical properties associated with spherical cavities versus elongated cracks in similar dimensions were not discussed in this study, but these findings could be highly significant for future research.

3.4 Microstructure and micro-hardness

It has been observed that the molten pool in the remelted samples is more homogeneous. However, metallographic images (Fig. 15) reveal that remelting, while potentially aiding in homogenizing the molten pool, may also penetrate other layers. This is evident in the metallographic images of the polished corner surface (along the printing axis) of the remelted sample (B). The black lines indicate the formation

of molten pools in each layer. The thickness of each of these layers is 30 μm, which is set prior to the start of printing. However, in certain regions, it can be seen that the molten pool has occasionally penetrated into other layers, which is attributed to the effects of remelting. This penetration of the molten material into the remaining layers may help fill any remaining voids or cavities.

The remelted samples exhibited significant grain growth compared to the samples without remelting, which can lead to increased corrosion susceptibility and ductility. This can be justified by the fact that the temperature gradient after laser scanning is very high, and austenitic grains have very limited opportunity for growth. However, remelting, being applied with lower power and immediately scanning the melted surface, reduces the cooling rate of the scanned surface, allowing the grains more time to grow. In contrast, in heat-treated samples, the molten pool is generally eliminated, and the austenitic grain structure undergoes significant growth due to the considerable time spent in the furnace.

The heat-affected zone in SLM is dependent on various parameters. The most important parameter, which not only affects the heat-affected zone but is also considered one of the main parameters of this process, determines the quality of the produced part from the aspect of relative density and integrity of the surface [40]. This parameter is the laser energy density, which is derived from the following equation.

$$\mathrm{Ev} = \frac{P}{v \times h \times t}$$

where v is scanning speed in mm/s, P is power in W, t is layer thickness in mm and h is hatch spacing in mm [35]. The Heat Affected Zone (HAZ) and laser energy density
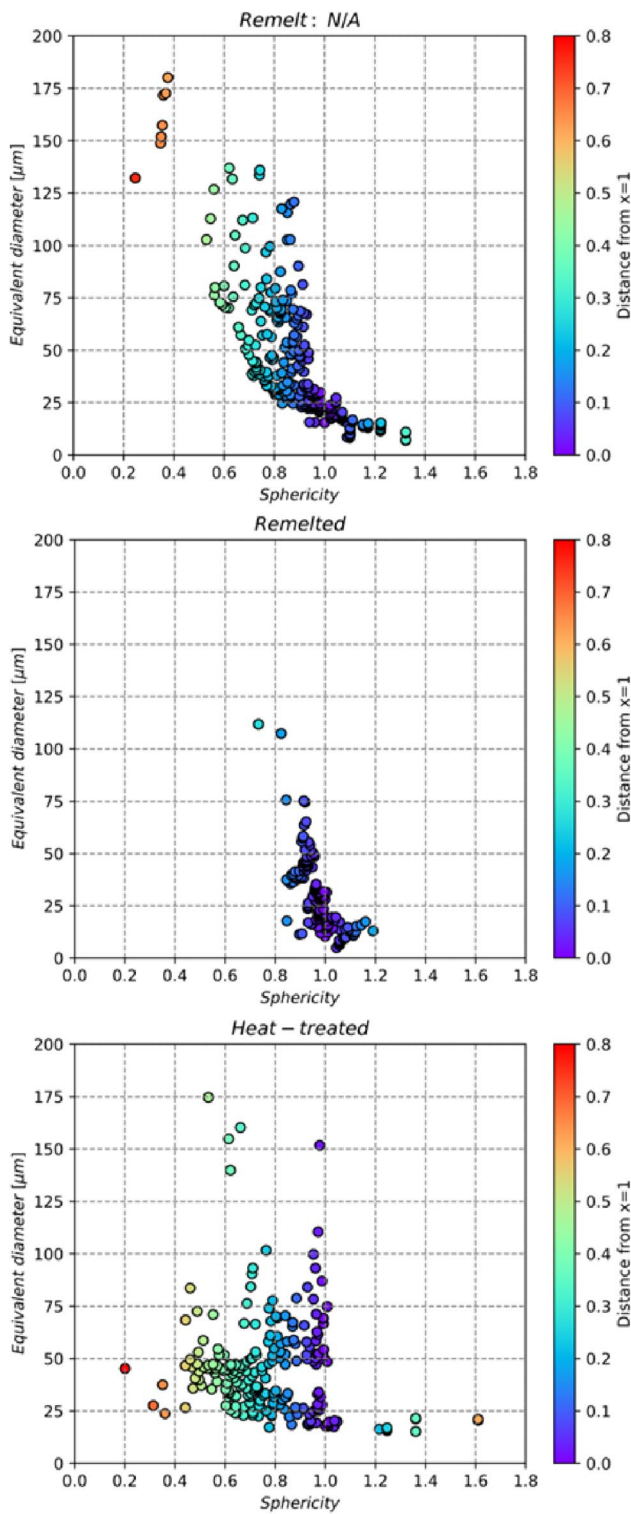
Fig. 14 Sphericity based on equivalent diameter for no-remelted, remelted and heat-treated samples

have a direct relationship. Therefore, with the increase in laser power and the reduction in scanning speed, the heat-affected zone becomes larger and hotter, which was a

conclusion reached by FEM modeling of this process. For example, for a laser power of 400 W and a scanning speed of 0.2 m/min, HAZ was approximately 2 mm, which is much larger than the thickness of a layer, allowing heat to penetrate into other layers [40].

In the context of initial melting and remelting, it is crucial to understand that remelting can significantly increase the heat-affected zone (HAZ), especially when conducted with the same laser power and scanning speed. This phenomenon is particularly relevant due to the immediate second scan occurring just before the addition of powder, which introduces more energy into the already melted layer. In our process optimization efforts, we have strategically reduced the remelting power and increased the scanning speed to mitigate overheating, minimize thermal gradients within the melt pool, and consequently, decrease the printing time. This adjustment has been instrumental in enhancing the efficiency and reliability of our selective laser melting (SLM) process. So it can be said that, the remelting strategy can cause a larger and deeper and even hotter HAZ compare to initial melting strategy, but investigating the actual size and properties of HAZ and determining all the influential parameters on this matter requires a separate research and advanced lab equipments in order to measure and analyze the absolute properties of HAZ.

By examining the hardness results of the remelted sample, it was found that in addition to an overall increase in hardness, it also exhibited a more homogeneous hardness distribution based on the two-dimensional hardness contours, with values ranging between 204 and 207 Vickers. The increase in hardness, even with the presence of larger grains, could be attributed to the improved microstructure, reduction in voids, and enhanced grain boundaries. In contrast, the sample without remelting had lower hardness and greater fluctuations in hardness values, ranging from 196.8 to 202.4. The hardness of the heat-treated sample, due to excessive grain growth, ranged from 170 to 171.6.

4 Conclusions

The objective of this research was to examine how surface roughness, relative density, and micro-hardness are affected by process parameters in Selective Laser Melting (SLM), a metal additive manufacturing technology. Specifically, the focus was on examining the remelting strategy and its compatibility with remelt interference parameters. The experimental design employed the Full Factorial method to systematically analyze the effects of various parameters. Surface roughness was quantified using a laser profilometer, while relative density was determined through micro-computed tomography (microCT). Furthermore, the obtained results were compared
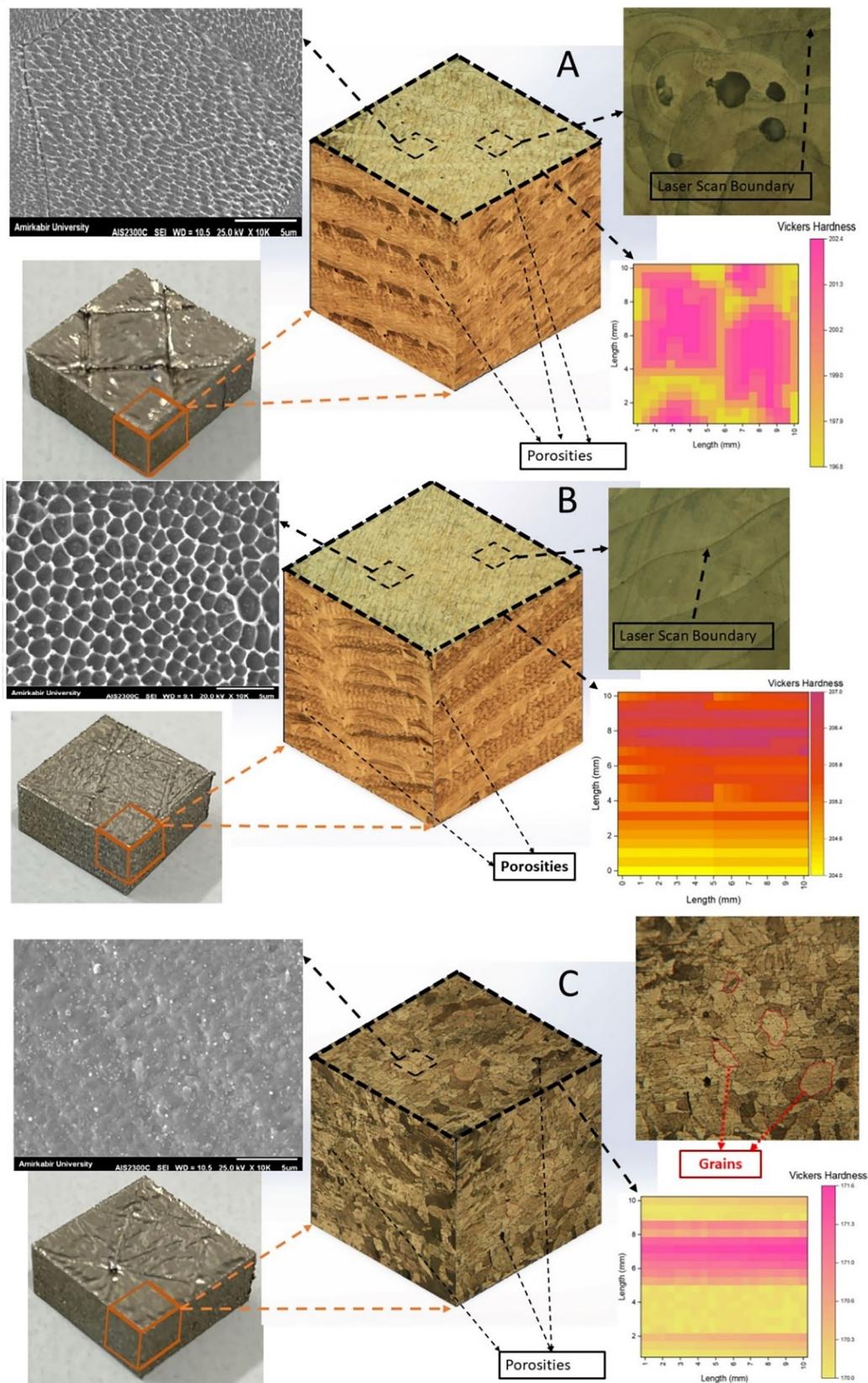
Fig. 15 Metallographic and SEM images of grain structure and surface microhardness contours from samples: **A** (No Remelted), **B** (Remelted), and **C** (Heat Treated)

with those achieved through post-processing techniques, namely sand blast and heat treatment (annealing), to assess their effectiveness.

- The findings indicate that the remelting parameter applied to the layers exerted the most pronounced influence on the surface roughness of the samples. However, no significant distinction in surface roughness was observed between remelting all layers concurrently or remelting every other layer. Consequently, to enhance surface roughness while concurrently mitigating costs and time requirements, the adoption of skip layer remelting is suggested.
- The surface roughness of the samples subjected to remelting was significantly superior to that achieved through the sandblast. The remelting strategy was capable of reducing surface roughness within a range of 7 μm, whereas sandblast achieved a reduction in surface roughness within a range of 11 to 13 μm.
- Remelting the layers, when combined with the optimal selection of other parameters, enhances the relative density and promotes uniformity within the melt pool. For instance, remelting all layers with a line spacing of 60 and 40 μm resulted in a decrease in relative density due to excessive heat generation in the melt pool region. However, a line spacing of 80 μm exhibited better compatibility and increased the relative density. On the other hand, employing a smaller line spacing suggests the adoption of skip layer remelting between the layers.
- The heat treatment (annealing) is capable of reducing smaller and spherical voids; however, it is ineffective in eliminating larger and elongated voids due to the nature of the process, which does not reach the melting point. Conversely, remelting, being an in-situ process strategy, offers more desirable outcomes such as higher relative density and reduced porosity, including the elimination of elongated and spherical voids, with significantly lower costs and time requirements.
- The occurrence of voids within the remelted sample was recorded as 161 instances, whereas in the non-remelted sample, the corresponding numbers were 329 and 221 for untreated and heat-treated samples, respectively.
- The diameter-equivalent plots based on sphericity clearly indicate that the average dimensions of elongated cavities are much larger than those of gas or spherical cavities.
- Remelting led to a more uniform microstructure, and despite grain growth, it resulted in an increase in hardness ranging from 202 to 207 Vickers.

It is recommended that future research examine the remelting approach (chessboard, minder, etc.) to determine the best one, as well as the effect of different types of porosity on mechanical strength in SLM-produced components

References

1. Hatami S et al (2020) Fatigue strength of 316 L stainless steel manufactured by selective laser melting. J Mater Eng Perform 29(5):3183–3194
2. Enneti RK, Morgan R, Atre SV (2018) Effect of process parameters on the Selective Laser Melting (SLM) of tungsten. Int J Refract Metal Hard Mater 71:315–319
3. Wang X, Gong X, Chou K (2016) Review on powder-bed laser additive manufacturing of Inconel 718 parts. Proc Inst Mech Eng Part B J Eng Manuf 231(11):1890–1903
4. Özakinci M, Ünal R (2023) the effect of scanning strategy on mechanical properties and delamination during brake caliper manufacturing with selective laser melting (SLM). J Polytech. https://doi.org/10.2339/politeknik.1214999
5. Kluczynski J et al (2020) Comparison of different heat treatment processes of selective laser melted steel based on analysis of mechanical properties. Materials 13:17
6. Nie H et al (2024) A new laser remelting strategy for direct energy deposition of 316L stainless steel. Proc Inst Mech Eng Part B J Eng Manuf. https://doi.org/10.1177/09544054231222047
7. Behera MP, Dougherty T, Singamneni S (2020) Selective laser melting of stainless steel and silicon nitride fibre metal matrix composites. Proc Inst Mech Eng Part B J Eng Manuf 234(12):1513–1525
8. Parikh Y, Kuttolamadom M (2023) Property-graded stainless steel 316l by selective laser melting: characterization & design. J Manuf Sci Eng 145(1):5
9. Khodabandeh A et al (2024) Surface integrity and fatigue behavior of AISI 4340 steel after hybrid laser-ultrasonic assisted ball burnishing process. Proc Inst Mech Eng C J Mech Eng Sci. https://doi.org/10.1177/14644207231196266
10. Sayadi D et al (2023) Using shot peening and burnishing to improve fatigue performance of additively manufactured 316L stainless steel. Proc Instit Mech Eng Part L J Mater Design Applic. https://doi.org/10.1177/14644207231196266
11. Majeed A et al (2020) Investigation of T4 and T6 heat treatment influences on relative density and porosity of AlSi10Mg alloy components manufactured by SLM. Comput Ind Eng. https://doi.org/10.1016/j.cie.2019.106194
12. Mugwagwa Y, Matope I, Matope S (2019) Effect of process parameters on residual stresses distortions, and porosity in selective laser melting of maraging steel 300. Metals. https://doi.org/10.3390/met9101042
13. Ali H et al (2017) In-situ residual stress reduction, martensitic decomposition and mechanical properties enhancement through high temperature powder bed pre-heating of Selective Laser Melted Ti6Al4V. Mater Sci Eng, A 695:211–220
14. Coeck S et al (2019) Prediction of lack of fusion porosity in selective laser melting based on melt pool monitoring data. Addit Manuf 25:347–356
15. Zhang C et al (2023) Characterization of porosity in lack of fusion pores in selective laser melting using the wavefunction. Mater Res Express. https://doi.org/10.1088/2053-1591/acaf24
16. Liu B et al (2022) Predicting the porosity defects in selective laser melting (SLM) by molten pool geometry. Int J Mech Sci. https://doi.org/10.1016/j.ijmecsci.2022.107478
17. Ye C et al (2021) Effects of post-processing on the surface finish, porosity, residual stresses, and fatigue performance of

additive manufactured metals: a review. J Mater Eng Perform 30(9):6407–6425

18. Chang S-J, Wei Z-X (2020) Influences of the scanning strategy on surface roughness in selective laser melting. Proc Inst Mech Eng Part B J Eng Manuf 236(14):1853–1866

19. Kaynak Y, Kitay O (2018) Porosity surface quality, microhardness and microstructure of selective laser melted stainless steel resulting from finish machining. J Manuf Mater Process. https://doi.org/10.3390/jmmp2020036

20. Nezarati M et al (2023) The effect of the vibratory surface finishing process on surface integrity and dimensional deviation of selective laser melted parts. Proc Inst Mech Eng Part B: J Eng Manuf. https://doi.org/10.1177/09544054231214016

21. Yasa E, Deckers J, Kruth JP (2011) The investigation of the influence of laser re-melting on density, surface quality and microstructure of selective laser melting parts. Rapid Prototyp J 17(5):312–327

22. Shin W-S et al (2021) Heat treatment effect on the microstructure, mechanical properties, and wear behaviors of stainless steel 316L prepared via selective laser melting. Mater Sci Eng. https://doi.org/10.1016/j.msea.2021.140805

23. Qin LY et al (2019) Microstructure homogenizations of Ti-6Al-4V alloy manufactured by hybrid selective laser melting and laser deposition manufacturing. Mater Sci Eng, A 759:404–414

24. Jiang R et al (2020) Effect of heat treatment on microstructural evolution and hardness homogeneity in laser powder bed fusion of alloy 718. Addit Manuf. https://doi.org/10.1016/j.optlastec.2022.108609

25. Feng Z et al (2022) Effect of heat treatment patterns on porosity, microstructure, and mechanical properties of selective laser melted TiB2/Al–Si–Mg composite. Mater Sci Eng. https://doi.org/10.1016/j.jmatprotec.2021.117386

26. Carson HC (2021) Heat treatments to improve microstructures of nickel alloys after selective laser melting

27. Ali H, Ghadbeigi H, Mumtaz K (2018) Effect of scanning strategies on residual stress and mechanical properties of Selective Laser Melted Ti6Al4V. Mater Sci Eng, A 712:175–187

28. Duan W, Wu M, Han J (2020) Effect of laser rescanning on Ti6Al4V microstructure during selective laser melting. Proc Inst Mech Eng Part B J Eng Manuf 235(5):763–771

29. Shao W et al (2022) Effect of hatch spacing and laser remelting on the formation of unique crystallographic texture of IN718 superalloy fabricated via laser powder bed fusion. Optics Laser Technol. https://doi.org/10.1016/j.optlastec.2022.108587

30. Han Q, Jiao Y (2019) Effect of heat treatment and laser surface remelting on AlSi10Mg alloy fabricated by selective laser melting. Int J Adv Manuf Technol 102(9–12):3315–3324

31. Liu B, Li B-Q, Li Z (2019) Selective laser remelting of an additive layer manufacturing process on AlSi10Mg. Results Phys 12:982–988

32. Gustmann T et al (2018) Selective laser remelting of an additively manufactured Cu-Al-Ni-Mn shape-memory alloy. Mater Des 153:129–138

33. Ma Y et al (2021) Effect of rescanning with reduced interlayer times on microstructure and properties of titanium alloy via selective laser melting. Proc Inst Mech Eng Part B J Eng Manuf 236(6–7):648–658

34. Gao B et al (2022) A review of research progress in selective laser melting (SLM). Micromachines 14:1

35. Mohseni M et al (2023) The effect of selective laser melting process parameters and remelting scanning strategy on relative density and surface hardness of stainless steel 316L. Proc Inst Mech Eng Part E J Process Mech Eng. https://doi.org/10.1177/09544089231207809

36. Qiu C et al (2019) Influence of laser processing strategy and remelting on surface structure and porosity development during selective laser melting of a metallic material. Metall Mater Trans A 50(9):4423–4434

37. Yasa E, Kruth JP (2011) Microstructural investigation of Selective Laser Melting 316L stainless steel parts exposed to laser re-melting. Proc Eng 19:389–395

38. Yu W et al (2019) Influence of re-melting on surface roughness and porosity of AlSi10Mg parts fabricated by selective laser melting. J Alloy Compd 792:574–581

39. Bakhtiarian M et al (2024) The effects of SLM process parameters on the relative density and hardness of austenitic stainless steel 316L. J Market Res 29:1616–1629

40. Mirkoohi E et al (2018) Thermal modeling of temperature distribution in metal additive manufacturing considering effects of build layers, latent heat, and temperature-sensitivity of material properties. J Manuf Mater Process 2(3):63